A threedimensional quantum mechanical study of the H2+H+ 2 system: Calculation of reactive and charge transfer cross sections

Michael Baer and Cheuk Y. Ng

Citation: The Journal of Chemical Physics **93**, 7787 (1990); doi: 10.1063/1.459359
View online: http://dx.doi.org/10.1063/1.459359
View Table of Contents: http://scitation.aip.org/content/aip/journal/jcp/93/11?ver=pdfcov
Published by the AIP Publishing

A three-dimensional quantum mechanical study of the $H_2 + H_2^+$ system: Calculation of reactive and charge transfer cross sections

Michael Baer[a] and Cheuk Y. Ng
Ames Laboratory, U.S. Department of Energy, Department of Chemistry, Iowa State University, Ames, Iowa 50011

(Received 4 June 1990; accepted 9 August 1990)

A three-dimensional quantum mechanical study of the $H_2 + H_2^+$ system is presented. The numerical study was carried out on the two lowest adiabatic surfaces, to permit charge transfer processes. All *seven* possible reactive arrangement channels were assumed to take part in the exchange process. The treatment was carried out within the framework of the rotational decoupling infinite order sudden approximation (IOSA). The reactive cross sections were compared both with surface hopping calculations and with experiment. Whereas the fit with experiment was reasonable, a less satisfactory fit was obtained with the semiclassical results. The analysis leads to the conclusion that the main source for the discrepancy are the nonadiabatic coupling terms which are included in the quantum mechanical treatment but ignored in the semiclassical treatment.

I. INTRODUCTION

$H_2 + H_2^+$ is a very important ion–molecule system, and probably the most important four-centered one. It has been the subject of a large number of experimental[1–6] and theoretical studies.[7–11] A characteristic of $H_2 + H_2^+$ is that both charge transfer (CT) and chemical exchange (atom or proton transfer) may take place during a collision, particularly in the low center-of-mass collision energy region $0 \leqslant E_{c.m.} \leqslant 1.0$ eV, where the competition between the two processes may lead to interesting results. The present study treats this energy range and therefore considers both processes.

To treat the reactive atom (ion) system, we employ the quantum mechanical (QM) approach which makes use of a new technique based on the negative imaginary decoupling potentials (NIDP).[12–17] Applying these potentials one can convert a multi-arrangement-channel system into an inelastic-single-arrangement system. By doing this one obtains not only all the *correct* S-matrix elements for the inelastic processes (which usually include all the CT processes), but also the *correct* total and sometimes even the state-to-state reactive probabilities and (integral) cross sections for all the ignored products arrangement channels. The conversion is done by attaching to each chemical bond expected to be broken during the collision a negative imaginary (complex) potential such that quantum fluxes generated by the rupture of this bond are smoothly absorbed, while the wave function in other regions (particularly in the intimately close interaction region and the exit arrangement channel) remains unaffected. So far we have treated a number of collinear and three-dimensional systems.[13–15] These treatments were carried out within the time-dependent wave packet framework[13] and the time-independent framework.[14,15]

Based on this new approach we performed two extensions. First, we developed a new version of a reactive infinite order sudden approximation (IOSA)[16,17] which performed much better than our previous version,[18] and secondly, we applied this new reactive IOSA to study the $(Ar + H_2)^+$ system for which we treated both the CT and the reactive processes.[17] The very nice agreement between the QM and the experimental results which we obtained for this system encouraged us to implement this approach in the $H_2 + H_2^+$ system.

At this stage we would like to refer to a collinear (time-independent) treatment for the $H + H_2$ system, in which the NIDP was conveniently applied.[15] In that work we showed that the Schrödinger equation (SE), which contained the complex potential [substituted along the bond of the reagent molecule (see Fig. 1)], could be solved without any difficulty by propagating the wave function from the origin to the asymptotic region, just as though an inelastic system were being treated (exactly the same recipe is followed). In addition, the parameters of the NIDP were determined *a priori*, based on analytic arguments, and the calculated transition probabilities were shown to be rather stable against reasonable variations of these parameters.

Although the introduction of NIDP's greatly reduces both the programming effort and the computer time consumption, still the (nonreactive) $H_2 + H_2^+$ system is too complicated to be treated without any approximation. Consequently, we propose an extended IOSA, in which three internal angles γ_{12}, γ_{34}, and ϕ (see Fig. 2) are held fixed, while the dynamics for r_{12}, r_{34}, and R is carried out. The resulting S-matrix elements, which depend on these three angles, are finally integrated with respect to them in order to obtain the physical S-matrix (or probability matrix) elements.

The reactive $H_2 + H_2^+$ system is a *seven*-arrangement system. This is best seen if one examines a general four-atom

[a] Visiting professor. Permanent address: Department of Physics and Applied Mathematics, Soreq Nuclear Research Center, Yavne 70600, Israel.

 0021-9606/90/237787-13$03.00

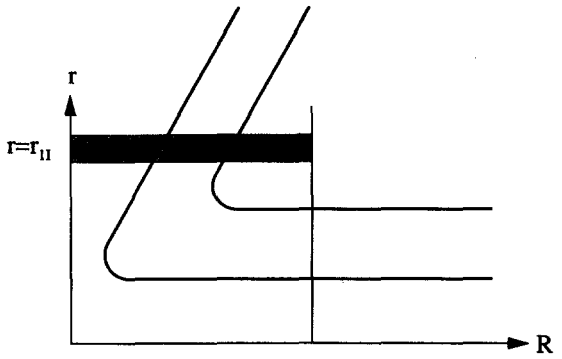

FIG. 1. The collinear (atom–diatom) type potential energy surface. The negative imaginary decoupling potential (NIDP) is located in the shadowed area.

system AB→CD and counts all the possible products:

$$AB + CD \rightarrow \begin{cases} ABC + D \\ ABD + C \\ A + BCD \\ B + ACD \\ AC + BD \\ AD + BC \end{cases}.$$

These seven arrangements are accessible in the low energy $H_2 + H_2^+$ and the formation of all six possible products is taken into account in our treatment. This is done, as mentioned above and as will be described in more detail in the next section, by attaching an NIDP to both the H_2 bond and the H_2^+ bond. It must be emphasized that, in our treatment, all four interacting particles are treated as distinguishable particles. Quantum mechanical reactive scattering studies which involve four atoms are scarce. It is only very recently that two such studies, for a collinear system in which all four atoms were assumed to be aligned along a straight line, appeared in print.[19] Although these studies led to some interesting results, the collinearity assumption was rather severe in that it eliminated five of the six possible product arrangement channels.

The potential used in the present treatment is essentially the semiempirical potential by Polak[20] (his type I potential), formulated within the diatomics-in-molecules (DIM).[21] The final outcome of Polak's treatment is an 8×8 diabatic potential matrix. In order to use this potential in our numerical treatment we reduced Polak's 8×8 potential matrix to a 2×2 diabatic potential matrix. We did this by employing the adiabatic–diabatic transformation angle α, which is obtained from the various nonadiabatic coupling terms.[22,23] Further details are given in Sec. II.

Existent theoretical studies of the $H_2 + H_2^+$ fall into two main categories, those concerning CT processes[7] and therefore emphasizing mainly the high energy region (which is beyond the scope of the present study), and those concerning the reaction process and therefore concentrating on the low-energy region.[8–11] To our knowledge, no detailed theoretical study has discussed both the reaction and the CT processes (a few results for these two processes were given by Muckerman[9] but no details or analysis were provided). So far, low-energy reactive studies of the $H_2 + H_2^+$ have been carried out employing the trajectory-surface-hopping method (TSHM), originally given for the atom–diatom case by Preston and Tully[24] and then extended[9–11] to a four-atom system. The most detailed studies of this system, which have relevance to ours, were carried out by Eaker and Schatz;[10,11] they will be discussed below.

The paper is organized in the following way: Sec. II is devoted to the theory and presents the four-atom system (in three dimensions), the NIDP, the reactive and CT IOSA-SE, and the adiabatic–diabatic transformation which leads to the 2×2 diabatic potential matrix. In Sec. III we comment on a few numerical aspects of this calculation. In Sec. IV we present the results, while in Sec. V we analyze and discuss them. A summary is given in Sec. VI.

II. THEORY

A. Introductory remarks

The theoretical treatment of ion–molecule collisions involving electronic transitions (i.e., electronic excitations and CT) is divided into two parts: (a) the potential energy surface (which is usually given in the form of a multidimensional DIM matrix), and the modifications which must be made in order to put it into a form appropriate for solving the SE; and (b) the treatment of the SE and the S-matrix elements to be calculated.

These two aspects have been discussed in several previous publications, particularly the potential energy surface, which involves the transition from the adiabatic to the diabatic representation. However, since this is our first study treating a four-atom (-ion) system and since the extension of our theory to this case is not always straightforward, we shall discuss it briefly here, leaving out the obvious details.

B. The four-atom (-ion) system

In order to treat a reactive system in our approach, we consider only one arrangement channel at a time. This we do by introducing the NIDP's, which reduce significantly the configuration space to be considered in a single calculation. We shall therefore limit this theoretical part to a discussion of the reagents arrangement, which is made up of two diatomic molecules. The four-atom system is described in Figs. 2(a) and 2(b). Six internal coordinates are required to describe the motion of the four-atom system. The most appropriate ones (for the reagents channel) are the following:

(1) The internal distance of the first diatomic r_{12}.
(2) The internal distance of the second diatomic r_{34}.
(3) The distance between the center of masses of the two diatomics R.
(4) The orientation angle γ_{12}, defined as

$$\gamma_{12} = \cos^{-1}(\hat{\mathbf{R}}\hat{\mathbf{r}}_{12}). \tag{2.1}$$

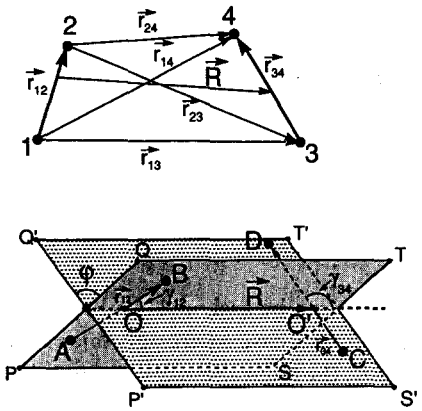

FIG. 2. The three-dimensional four-atom system. (a) The six interatomic vectors. (b) The two intersecting planes for the four-atom system. PQST is the plane which contains the diatomic molecule AB and the center of mass of the CD diatomic; P'Q'S'T' is the plane which contains CD and the center of mass of AB. The intersection line is the translational vector R, which lies in both planes. Also shown are the three IOSA angles γ_{12}, γ_{34}, and ϕ.

(5) The orientation angle γ_{34}, defined as

$$\gamma_{34} = \cos^{-1}(\hat{\mathbf{R}}\hat{\mathbf{r}}_{34}). \tag{2.2}$$

(6) The angle ϕ, which is the angle between the $(\hat{\mathbf{R}},\hat{\mathbf{r}}_{12})$ and the $(\hat{\mathbf{R}},\hat{\mathbf{r}}_{34})$ planes.

With the help of γ_{12}, γ_{34} and ϕ we are able to calculate the angle δ, which is defined as the angle between $\hat{\mathbf{r}}_{12}$ and $\hat{\mathbf{r}}_{34}$:

$$\delta = \cos^{-1}(\cos\gamma_{12}\cos\gamma_{34} + \sin\gamma_{12}\sin\gamma_{34}\cos\phi). \tag{2.3}$$

Once the three vectors $\mathbf{R}_{12}$, $\mathbf{r}_{12}$, and $\mathbf{r}_{34}$ are given, all the other interatomic vectors $\mathbf{r}_{13}$, $\mathbf{r}_{24}$, $\mathbf{r}_{23}$, and $\mathbf{r}_{14}$ can be presented as the following linear combinations:

$$\mathbf{r}_{ij} = \mathbf{R} + \Gamma_{12,i}\mathbf{r}_{12} + \Gamma_{34,j}\mathbf{r}_{34}, \tag{2.4}$$

where

$$\Gamma_{12,i} = \delta_{i1} - \frac{m_1}{m_1+m_2}, \qquad \Gamma_{34,j} = \delta_{j4} - \frac{m_4}{m_3+m_4}. \tag{2.5}$$

Squaring Eq. (2.4) yields the expression for the distances between the i and the j atoms:

$$r_{ij} = \{R^2 + \Gamma_{12,i}^2 r_{12}^2 + \Gamma_{34,j}^2 r_{34}^2 + 2Rr_{12}\Gamma_{12,i}\cos\gamma_{12} + 2Rr_{34}\Gamma_{34,j}\cos\gamma_{34} + 2r_{12}r_{34}\Gamma_{12,i}\Gamma_{34,j}\cos\delta\}^{1/2}. \tag{2.6}$$

Finally, we introduce the following partial derivatives, which are required later to calculate the adiabatic–diabatic transformation angle α. Thus,

$$\frac{\partial r_{ij}}{\partial R} = \frac{1}{r_{ij}}(R + r_{12}\Gamma_{12,i}\cos\gamma_{12} + r_{34}\Gamma_{34,j}\cos\gamma_{34}),$$

$$\frac{\partial r_{ij}}{\partial r_{12}} = \frac{1}{r_{ij}}(\Gamma_{12,i}^2 r_{12} + R\Gamma_{12,i}\cos\gamma_{12} + r_{34}\Gamma_{12,i}\Gamma_{34,j}\cos\delta), \tag{2.7}$$

$$\frac{\partial r_{ij}}{\partial r_{34}} = \frac{1}{r_{ij}}(\Gamma_{34,j}^2 r_{34} + R\Gamma_{34,j}\cos\gamma_{34} + r_{12}\Gamma_{12,i}\Gamma_{34,j}\cos\delta).$$

Equations (2.7) only hold for r_{13}, r_{14}, r_{23}, and r_{24}. Since we consider only the reagents channel, the mass scaling which is usually done for reactive systems becomes redundant and therefore our discussion of the four-atom system coordinates is ended at this stage.

C. The potential

The potential energy surface used in this calculation is the DIM potential[21] as originally constructed by Polak[20] (his type I surface) and somewhat modified by Eaker and Schatz[10,11] (this surface is similar to that employed by Stine and Muckerman).[9] The DIM prescription leads to an 8×8 matrix the two lowest eigenvalues of which define the two required adiabatic potential energy surfaces. In addition, employing the Hellman–Feynman theorem,[23] we get the required nonadiabatic coupling terms, which are responsible for the coupling between these two adiabatic surfaces. The features of the resultant surfaces have already been discussed several times and will therefore be mentioned here only very briefly.

The potentials (and the nonadiabatic coupling terms) are not in a form suitable for performing the quantum mechanical dynamic calculations, mainly because of the vibrational nonadiabatic coupling terms, which become δ functions once the translational coordinate becomes large.[23] In order to avoid this difficulty, it is necessary to perform a transformation from the adiabatic to the diabatic representation; this not only eliminates the spiky nonadiabatic coupling terms but also yields the correct physical representation of the asymptotic (diatomic) potentials. This transformation has already been described for an atom–diatom case,[23] and will be repeated here because now it is applied to a diatom–diatom case, which is somewhat different.

The main difference between the two cases is related to the *seam*. In the collinear atom–diatom system, the seam is a line

$$r = r(R) \tag{2.8}$$

along which the two *diabatic* surfaces cross. In most cases studied so far, i.e., in $Ar^+ + H_2$, $Ar + H_2^+$,[7,26] $H^+ + H_2(D_2,HD)$,[25,27] the seam follows an almost *straight* line along the entrance arrangement channels (and sometimes along the exit channel too). A similar line is found to exist in the three-dimensional case. In the diatom–diatom case, the crossing takes place whenever r_{12} becomes equal to r_{34}, independent of the value of R or other geometrical magnitudes.[9,10] This observation will help in the calculation of the adiabatic–diabatic transformation angle α.

The transformation from the adiabatic to the diabatic representation is carried out via an orthogonal transformation matrix $\mathbf{A}$.[22,23,28] Thus, if $\mathbf{V}$ is the 2×2 *adiabatic* poten-

tial matrix, then **W**, the 2×2 corresponding *diabatic* potential matrix, is given in the form

$$\mathbf{W}=\mathbf{A}^*\mathbf{V}\mathbf{A}, \tag{2.9}$$

where **A** fulfills the vectorial differential equation:

$$\nabla\mathbf{A}+\boldsymbol{\tau}^{(1)}\mathbf{A}=0. \tag{2.10}$$

Here ∇ stands for the six-component vectorial operator:

$$\nabla=\left(\frac{\partial}{\partial r_{12}},\frac{\partial}{\partial r_{13}},\frac{\partial}{\partial r_{14}},\frac{\partial}{\partial r_{23}},\frac{\partial}{\partial r_{24}},\frac{\partial}{\partial r_{34}}\right) \tag{2.11}$$

and $\boldsymbol{\tau}^{(1)}$ is a six-component vector of 2×2 antisymmetrical matrices of the kind

$$\boldsymbol{\tau}_{ij}^{(1)}=\begin{pmatrix}0 & \tau_{ij}^{(1)}\\ -\tau_{ij}^{(1)} & 0\end{pmatrix};\quad i<j,\ i,j=1,2,4. \tag{2.12}$$

The matrix elements $\tau_{ij}^{(1)}$ are the nonadiabatic coupling terms obtained from the DIM matrix, employing the Hellman–Feynman theorem.[23] Consequently, for each i and j $(i\neq j)$, **A** has to fulfill the equation

$$\left(\mathbf{I}\frac{\partial}{\partial r_{ij}}+\boldsymbol{\tau}_{ij}^{(1)}\right)\mathbf{A}=0. \tag{2.13}$$

Instead of using the interatomic distance, we can express the vectorial equation (2.10) in terms of the six Jacobi coordinates $(R, r_{12}, r_{34}, \gamma_{12}, \gamma_{34}, \phi)$.

As mentioned in the Introduction, the present treatment is carried out within the framework of the IOSA employed with respect to the three angles γ_{12}, γ_{34} and ϕ. Consequently, like in the atom–diatom case,[17,25] the six-component-vector equation reduces to a three-(component) equation:

$$\begin{aligned}&\frac{\partial\mathbf{A}}{\partial R}+\boldsymbol{\tau}_R^{(1)}\mathbf{A}=0,\\ &\frac{\partial\mathbf{A}}{\partial r_{12}}+\boldsymbol{\tau}_{r_{12}}^{(1)}\mathbf{A}=0,\\ &\frac{\partial\mathbf{A}}{\partial r_{34}}+\boldsymbol{\tau}_{r_{34}}^{(1)}\mathbf{A}=0,\end{aligned} \tag{2.14}$$

where $\boldsymbol{\tau}_R^{(1)}$, $\boldsymbol{\tau}_{r_{12}}^{(1)}$ and $\boldsymbol{\tau}_{r_{34}}^{(1)}$ matrix elements are calculated from the previous $\boldsymbol{\tau}_{r_{ij}}^{(1)}$ matrix elements employing the chain rule for the derivatives. Thus,

$$\tau_x^{(1)}=\sum_{i,j}\tau_{r_{ij}}^{(1)}\frac{\partial r_{ij}}{\partial x};\quad x=R,\ r_{12},\ r_{34}, \tag{2.15}$$

where the $\partial r_{ij}/\partial x$'s; $x=R$, r_{12}, r_{34} are given in Eq. (2.7). Next, since **A** is a 2×2 orthogonal matrix, it can be written as

$$\mathbf{A}=\begin{pmatrix}\cos\bar{\alpha}, & -\sin\bar{\alpha}\\ \sin\bar{\alpha}, & \cos\bar{\alpha}\end{pmatrix}, \tag{2.16}$$

where, following Eq. (2.14), $\bar{\alpha}$ can be shown to fulfill the equations[23]

$$\frac{\partial\bar{\alpha}}{\partial x}+\tau_x^{(1)}\bar{\alpha}=0;\quad x=R,r_{12},r_{34} \tag{2.17}$$

[here $\tau_x^{(1)}$ is the matrix element given in Eq. (2.15)] and the solution for these three equations can be written in the form of a line integral:[22,23]

$$\begin{aligned}\bar{\alpha}(R,r_{12},r_{34})=&\bar{\alpha}(R_0,r_{12,0},r_{34,0})\\ &+\int_{R_0}^{R}dR\,\tau_R^{(1)}(R,r_{12,0},r_{34,0})\\ &+\int_{r_{12,0}}^{r_{12}}dr_{12}\,\tau_{r_{12}}^{(1)}(R,r_{12},r_{34,0})\\ &+\int_{r_{34,0}}^{r_{34}}dr_{34}\,\tau_{r_{34}}^{(1)}(R,r_{12},r_{34}),\end{aligned} \tag{2.18}$$

where $\bar{\alpha}_0=\bar{\alpha}(R_0,r_{12,0},r_{34,0})$ can be assigned any value but is usually chosen to be zero. In the case where only one crossing takes place for a given R, the angle α is expected to fulfill the relation

$$0\leqslant\bar{\alpha}\leqslant\pi/2. \tag{2.19}$$

Examples for $\bar{\alpha}$ functions are shown in Fig. 3. In the actual calculation, Eq. (2.18) had to be modified in the following way:

$$\begin{aligned}\alpha(R,r_{12},r_{34})=&\alpha_0(R)+\int_{r_{12,0}}^{r_{12}}dr_{12}\,\tau_{12}^{(1)}(R,r_{12},r_{34,0})\\ &+\int_{r_{34,0}}^{r_{34}}dr_{34}\,\tau_{34}^{(1)}(R,r_{12},r_{34}),\end{aligned} \tag{2.18'}$$

where $\alpha_0(R)$ is chosen in such a way that for each value R there is a point $(R,r_{12}=r_{12}^{(a)},r_{34}=r_{34}^{(a)})$ so that the value of $\alpha(R,r_{12}^{(a)},r_{34}^{(a)})$ is equal to zero. Such a choice of $\alpha_0(R)$ guarantees, as will be shown next, that the proposed transformation maintains, at least at one point for each given value of R, the adiabatic character of the surfaces (which are the physical potential energy surfaces). In this way some arbitrariness is introduced in the definition of the potential energy surfaces used in the calculations, but we found that, as long

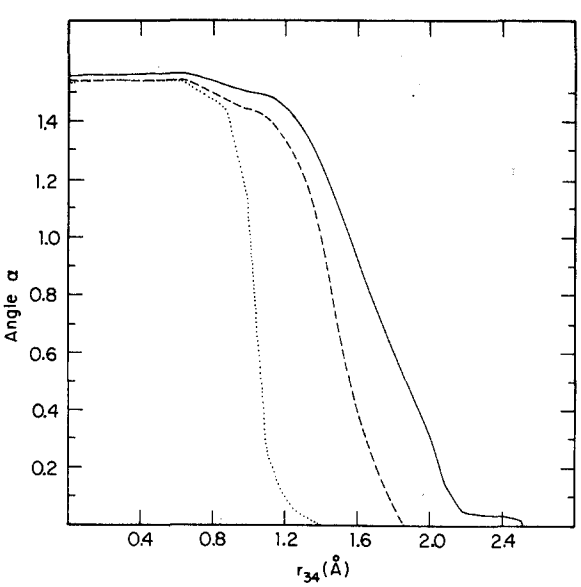

FIG. 3. The adiabatic–diabatic transformation angle calculated for $\gamma_{12}=0°$, $\gamma_{34}=90°$, $R=4$ Å, and three values of r_{12}, as a function of r_{34} (the H_2^+ vibrational coordinate). ···, $r_{12}=1.029$ Å; ---, $r_{12}=1.482$ Å; —, $r_{12}=2.274$ Å.

as one makes reasonable choices for $r_{12}^{(a)}$ and $r_{34}^{(a)}$ (namely, far enough from the seam, etc.), the results hardly change.

Having calculated $\alpha(R,r_{12},r_{34})$, we give the diabatic potential energy surfaces in the form

$$W_1 = V_1 \cos^2\alpha + V_2 \sin^2\alpha, \tag{2.20a}$$

$$W_2 = V_1 \sin^2\alpha + V_1 \cos^2\alpha, \tag{2.20b}$$

and the corresponding diabatic coupling term W_{12} becomes

$$W_{12} = \tfrac{1}{2}\sin 2\alpha(V_2 - V_1). \tag{2.20c}$$

It is now seen from Eqs. (2.20) that making $\alpha(R,r_{12},r_{34})$ equal to zero at $(R,r_{12}=r_{12}^{(a)},r_{34}=r_{34}^{(a)})$ yields the adiabatic surfaces at that point and a zero value for the corresponding diabatic coupling term.

Next, we consider the asymptotic region. Since as $R\to\infty$ the vibrational nonadiabatic coupling term becomes a δ function,[23] the transformation angle α becomes a step function:

$$\alpha(R=\infty;r_{12},r_{34}) = \begin{cases} \pi/2, & r_{12} > r_{34} \\ 0, & r_{12} < r_{34} \end{cases}. \tag{2.21}$$

This asymptotic behavior of α guarantees the correct asymptotic limit of the potential when the distance between the two diatomics becomes very large; in other words, it yields the correct diatomic potentials of the two molecules. Thus,

$$W_1(R=\infty;r_{12},r_{34}) = \begin{cases} V_1, & 0\leqslant r_{12}\leqslant r_{34} \\ V_2, & r_{12}\geqslant r_{34}\geqslant 0 \end{cases}, \tag{2.22a}$$

$$W_2(R=\infty,r_{12},r_{34}) = \begin{cases} V_1, & r_{12}\geqslant r_{34}\geqslant 0 \\ V_2, & 0\leqslant r_{12}\geqslant r_{34} \end{cases}. \tag{2.22b}$$

In addition, we have

$$W_{12}(R=\infty,r_{12},r_{34})\equiv 0. \tag{2.22c}$$

As was mentioned earlier, the actual scattering calculations are carried out for a given set of angles γ_{12}, γ_{34} and ϕ, which means that in the IOSA-SE are substituted the diabatic potentials $W_i(R,r_{12},r_{34};\gamma_{12},\gamma_{34},\phi)$; $i=1,2$ and the diabatic coupling term $W_{12}(R,r_{12},r_{34};\gamma_{12},\gamma_{34},\phi)$. In this presentation, the angle between the H_2 axis and R is γ_{12} and the angle between the H_2^+ axis and R is γ_{34} (see Fig. 2). However, while the two diatomics approach each other, the charge may move from one molecule to the other, which means that γ_{12} is now the angle between H_2^+ and R, and γ_{34} is the angle between H_2 and R. Consequently, the diabatic potentials become $W_i = W_i(R,r_{12},r_{34};\gamma_{34},\gamma_{12},\phi)$ [and the diabatic coupling term becomes $W_{12}=W_{12}(R,r_{12},r_{34};\gamma_{34},\gamma_{12},\phi)$]. However, the two sets of potentials, i.e., $W_i(R,r_{12},r_{34};\gamma_{12},\gamma_{34},\phi)$; $i=1,2$ and $W_{12}(R,r_{12},r_{34};\gamma_{12},\gamma_{34},\phi)$; $i=1,2$ are entirely different. For example, in Fig. 4 are presented the potentials along the minimum energy path for the two "twin" configurations, $(\gamma_{12}=0°,\gamma_{34}=90°)$ and $(\gamma_{12}=90°,\gamma_{34}=0°)$. It can be seen that the (0°, 90°) configuration is much more exothermic, and it is obvious that the system will follow the (lower) potential. Thus, while propagating the solution, we could calculate at each step the potentials for the two possible configurations $(\gamma_{12},\gamma_{34})$ and $(\gamma_{34},\gamma_{12})$ and choose the lower one (together with the corresponding upper one and the diabatic coupling term). Of course, in the asymptotic regions,

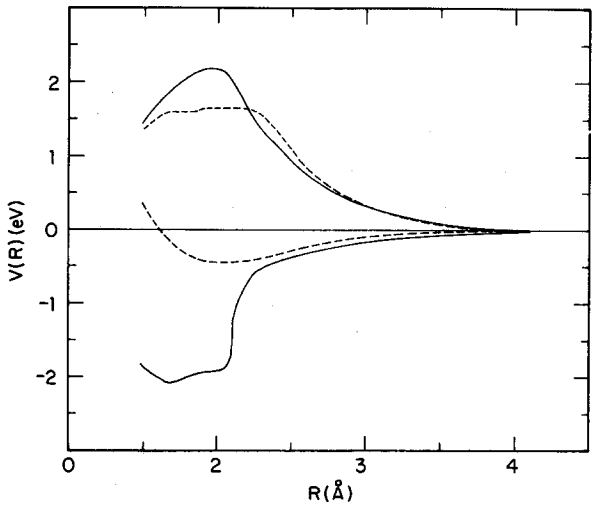

FIG. 4. The two lowest adiabatic–diabatic potentials along the minimum energy path, as calculated for the two "twin" configurations $\gamma_{12}=0°$, $\gamma_{34}=90°$ (—) and $\gamma_{12}=90°$, $\gamma_{34}=0°$ (---).

the two potentials $W_i(R,r_{12},r_{34};\gamma_{12},\gamma_{34},\phi)$ and $W_i(R,r_{12},r_{34};\gamma_{34},\gamma_{12},\phi)$; $i=1,2$ coincide. The actual calculations were done in a slightly different manner. Before starting to solve the SE we compared the potentials for the two given configurations and chose the lower one for the whole calculation.

D. The Schrödinger equation and the IOSA

As was mentioned above, within this new (reactive) IOSA we consider only the reagents arrangement channel. All other arrangement channels are eliminated, as will be explained below, by the use of NIDP. The fact that the products arrangements can be ignored enables the application of the ordinary inelastic (nonreactive) charge-transfer IOSA. However, this does not mean that the reactive cross sections cannot be obtained. On the contrary, like in our previous treatments,[12–17] we still calculate reactive probabilities and cross sections. These could, in principle, be calculated separately for each possible product, but we are mainly interested in the total reactive probability.

The treatment of an inelastic collision within the IOSA is well known and will be only briefly discussed here (see Ref. 26 for the treatment of a CT process within the IOSA). The only difference between the ordinary inelastic treatment and the treatment suggested here (see also Refs. 15 and 16) for a reactive system is the inclusion of the NIDP, and this is the subject we discuss next.

1. The negative imaginary decoupling potential (NIDP)

For an exchange to take place during a collision between two diatomic molecules at least one bond (and sometimes both bonds) have to be broken, which means that, following the reaction, the corresponding vibrational coordinate r becomes infinitely large. Thus, to each bond is attached a negative imaginary absorbing potential of the kind

$$u_I(r,x)=\begin{cases}-iu_{I0}(x)\dfrac{r-r_I}{\Delta r_I}; & r_I\leqslant r\leqslant r_I+\Delta r_I\\ 0; & \text{otherwise}\end{cases}, \tag{2.23}$$

where x stands for all other coordinates, r_I, $r_I+\Delta r_I$ is the range for which $u_I(r,x)$ is different from zero (r_I is usually chosen large enough so that the wave function, in the strong interaction region, is not affected by the introduction of the imaginary potential) and $u_{I0}(x)$ and Δr_I must be chosen in such a way that they fulfill the two inequalities:[12]

$$\hbar E_{\text{c.m.}}^{1/2}/(\Delta r_I\sqrt{8m})\ll u_{I0}(x)\ll\Delta r_I\sqrt{8m}E_{\text{c.m.}}^{3/2}/\hbar. \tag{2.24}$$

Here $E_{\text{c.m.}}$ stands for the translational energy of the system which interacts with the $u_I(r,x)$ and m is its mass. In Eq. (2.24), the left-hand inequality guarantees that all the flux passing through this potential is absorbed and the right-hand inequality guarantees that no flux is reflected while the wave function passes through the potential. As already mentioned, we associate each (reagents) bond with such a potential (in the present study we have two such bonds). Once these potentials are determined, we add them to the ordinary potential which governs the motion of the interacting particles and solve the SE in the usual way, except that now the potential is complex instead of being real. This fact did not introduce any essential difficulties.

2. The Schrödinger equation for a diatom–diatom system within the IOSA

Inelastic collisions within the IOSA which involve four atoms or more have been discussed several times in the past.[29,30] The relevant SE which describes the interaction between two diatomic molecules is written in the form:

$$\left\{-\frac{\hbar^2}{2\mu}\frac{\partial^2}{\partial R^2}-\frac{\hbar^2}{2m_{12}}\frac{\partial^2}{\partial r_{12}^2}-\frac{\hbar^2}{2m_{34}}\frac{\partial^2}{\partial r_{34}^2}+\frac{\hbar^2}{2\mu}\frac{l(l+1)}{R^2}+\frac{\hbar^2}{2m_{12}}\frac{j_{12}(j_{12}+1)}{r_{12}^2}+\frac{\hbar^2}{2m_{34}}\frac{j_{34}(j_{34}+1)}{r_{34}^2}+V_C(R,r_{12},r_{34};\gamma_{12},\gamma_{34},\phi)-E\right\}\times\Psi(R,r_{12},r_{34};\gamma_{12},\gamma_{34},\phi)=0, \tag{2.25}$$

where μ, m_{12}, m_{34} are the reduced masses given in the form

$$\mu=\frac{(m_1+m_2)(m_3+m_4)}{m_1+m_2+m_3+m_4};\quad m_{ij}=\frac{m_im_j}{m_i+m_j};\quad i=1,3,\ j=2,4. \tag{2.26}$$

l, j_{12}, and j_{34} are the orbital and the internal angular momentum quantum numbers, E is the total energy, and $V_c(R,r_{12},r_{34};\gamma_{12},\gamma_{34},\phi)$ is the complex potential:

$$V_c(R,r_{12},r_{34};\gamma_{12},\gamma_{34},\phi)=V(R,r_{12},r_{34};\gamma_{12},\gamma_{34},\phi)+u_{I12}(r_{12})+u_{I34}(r_{34}). \tag{2.27}$$

To study charge transfer, Eq. (2.25) must be extended in the form

$$\left\{\left[-\frac{\hbar^2}{2\mu}\frac{\partial^2}{\partial R^2}-\frac{\hbar^2}{2m_{12}}\frac{\partial^2}{\partial r_{12}^2}-\frac{\hbar^2}{2m_{34}}\frac{\partial^2}{\partial r_{34}^2}+\frac{\hbar^2}{2\mu}\frac{l(l+1)}{R^2}+\frac{\hbar^2}{2m_{12}}\frac{j_{12}(j_{12}+1)}{r_{12}^2}+\frac{\hbar^2}{2m_{34}}\frac{j_{34}(j_{34}+1)}{r_{34}^2}-E\right]\mathbf{I}+\mathbf{V}_c\right\}\Psi=0, \tag{2.28}$$

where $\mathbf{V}_c$ is now a 2×2 (diabatic) potential energy surface matrix, $\mathbf{I}$ is the unity matrix, and Ψ is a column vector with two components Ψ_1 and Ψ_2. It is important to emphasize that in the (H_2,H_2^+) system, only the lowest surface is reactive, and consequently the NIDP's are added only to $V_1(R,r_{12},r_{34};\gamma_{12},\gamma_{34},\phi)$.

Below we assume $j_{12}=j_{34}=0$ and consequently Eq. (2.28) becomes

$$\left\{\left[-\frac{\hbar^2}{2\mu}\frac{\partial^2}{\partial R^2}-\frac{\hbar^2}{2m_{12}}\frac{\partial^2}{\partial r_{12}^2}-\frac{\hbar^2}{2m_{34}}\frac{\partial^2}{\partial r_{34}^2}+\frac{\hbar^2}{2\mu}\frac{l(l+1)}{R^2}-E\right]\mathbf{I}+\mathbf{V}_C\right\}\Psi=0. \tag{2.29}$$

To solve Eq. (2.29), we divide the whole R range into N sectors (where $N\sim250$) and treat each sector separately, employing the close-coupling technique. A description of this approach (which is rather common) was given in one of our recent publications,[15] in which we describe in detail how the propagation of the solution of the SE is done for a complex potential. Here we shall only point out the details relating to the diatom–diatom case.

Considering an arbitrary sector with the midpoint $R=\bar{R}$, the wave functions $\Psi^{(i)}(R,r_{12},r_{34})$; $i=1,2$ are expanded in terms of two basis sets, one defined with respect to the coordinate r_{12} and the other with respect to r_{34} [in the following the index 1 will replace (12) and the index 3 will replace (34); also, whenever possible, we delete the three angles γ_1, γ_3, ϕ]:

$$\Psi^{(i)}(R,r_1,r_3)=\sum_{n_1,n_3}\psi_{n_1,n_3}^{(i)}(R)\phi_{n_1}^{(i)}(r_1|\bar{R},r_{30}^{(i)})\phi_{n_3}^{(i)}(r_3|\bar{R},r_{10}^{(i)});\quad i=1,2 \tag{2.30}$$

where $r_{10}^{(i)}$ and $r_{30}^{(i)}$ are the r_1 and r_3 values for which the i-th potential attains its minimum assuming $R=\bar{R}$, and $\phi_{n_{ji}}^{(i)}(r_j|\bar{R},r_{j0}^{(i)})$ are the eigenfunctions for the eigenequation:

$$\left[-\frac{\hbar^2}{2m_j}\frac{\partial^2}{\partial r_j^2}+V_i(\bar{R},r_j,r_{j'0})-\epsilon_{n_{ji}}^{(i)}(\bar{R},r_{j'0})\right]\times\phi_{n_{ji}}^{(i)}(r_j|\bar{R},r_{j,0}^{(i)})=0;\quad i=1,2,\ j=1,3,\ j'=3,1. \tag{2.31}$$

Here n_{ji} means that the vibrational quantum number n_j is related to the surface i and $\epsilon_{n_{ji}}^{(i)}$ is the corresponding eigenvalue. Defining the interaction potential $U_{ic}(R,r_1,r_3)$, $i=1,2$, as

$$U_{ic}(R,r_1,r_3)=V_{ic}(R,r_1,r_3)-V_i(\bar{R},r_1,r_{30})-V_i(\bar{R},r_{10},r_3);\quad i=1,2 \tag{2.32}$$

leads to the following coupled system of differential equations:

$$\left(-\frac{\hbar^2}{2\mu}\frac{\partial^2}{\partial R^2}+\frac{\hbar^2}{2\mu}\frac{l(l+1)}{R^2}+\epsilon^{(1)}_{n_{11}}+\epsilon^{(1)}_{n_{31}}-E\right)\psi^{(1)}_{n_{11}n_{31}}$$
$$+\sum_{n'_{11}n'_{31}}\langle n_{11}n_{31}|U_{1c}|n'_{11}n'_{31}\rangle\psi^{(1)}_{n'_{11}n'_{31}}$$
$$+\sum_{n'_{12}n'_{32}}\langle n_{11}n_{31}|V_{12}|n'_{12}n'_{32}\rangle\psi^{(2)}_{n'_{12}n'_{32}}=0, \quad (2.33)$$

$$\left(-\frac{\hbar^2}{2\mu}\frac{\partial^2}{\partial R^2}+\frac{\hbar^2}{2\mu}\frac{l(l+1)}{R^2}+\epsilon^{(2)}_{n_{12}}+\epsilon^{(2)}_{n_{32}}-E\right)\psi^{(2)}_{n_{12}n_{32}}$$
$$+\sum_{n'_{12}n'_{32}}\langle n_{12}n_{32}|U_{2c}|n'_{12}n'_{32}\rangle\psi^{(2)}_{n'_{12}n'_{32}}$$
$$+\sum_{n'_{11}n'_{31}}\langle n_{12}n_{32}|V_{12}|n'_{11}n'_{31}\rangle\psi^{(1)}_{n'_{11}n'_{31}}=0, \quad (2.34)$$

where

$$\langle n_{1i}n_{3i}|U_{ic}|n'_{1i}n'_{3i}\rangle$$
$$=\int\int dr_1\,dr_3\,\phi^{(i)}_{n_{1i}}(r_1|\bar{R},r^{(i)}_{30})\phi^{(i)}_{3i}(r_3|\bar{R},r^{(i)}_{10})$$
$$\times U_{ic}(R,r_1,r_3)\phi^{(i)}_{n'_{1i}}(r_1|\bar{R},r^{(i)}_{30})\phi^{(i)}_{n_{3i}}(r_3|\bar{R},r^{(i)}_{10});$$
$$i=1,2 \quad (2.35)$$

and

$$\langle n_{11}n_{31}|V_{12}|n'_{12}n'_{32}\rangle$$
$$=\int\int dr_1\,dr_3\,\phi^{(1)}_{n_{11}}(r_1|\bar{R},r^{(1)}_{30})\phi^{(1)}_{31}(r_3|\bar{R},r^{(1)}_{10})$$
$$\times V_{12}(R,r_1,r_3)\phi^{(2)}_{n'_{12}}(r_1|\bar{R},r^{(2)}_{30})\phi^{(2)}_{n_{32}}(r_3|\bar{R},r^{(2)}_{10}).$$
$$(2.36)$$

Equations (2.33) and (2.34) can be written in a slightly different form by defining the following matrix elements:

$$\langle n_{1i}n_{3i}|W_{ic}|n'_{1i}n'_{3i}\rangle=\frac{2\mu}{\hbar^2}\left[\langle n_{1i}n_{3i}|U_{ic}|n'_{1i}n'_{3i}\rangle\right.$$
$$\left.+V_i(\bar{R},r^{(i)}_{10},r^{(i)}_{30})\delta_{n_{1i}n'_{1i}}\delta_{n_{3i}n'_{3i}}\right];$$
$$i=1,2, \quad (2.37)$$

$$\langle n_{1i}n_{3i}|I_i|n'_{1i}n'_{3i}\rangle=\delta_{n_{1i}n'_{1i}}\delta_{n_{3i}n'_{3i}};\quad i=1,2, \quad (2.38)$$

$$\langle n_{1i}n_{3i}|k^{(2)}_i|n'_{1i}n'_{3i}\rangle=k^{(i)2}_{n_{1i}n_{3i}}\delta_{n_{1i}n'_{1i}}\delta_{n_{3i}n'_{3i}};\quad i=1,2, \quad (2.39)$$

where

$$k^{(i)}_{n_{1i}n_{3i}}=\left\{\frac{2\mu}{\hbar^2}\left[E-\epsilon^{(i)}_{n_{1i}}-\epsilon^{(i)}_{n_{3i}}+V_i(\bar{R},r^{(i)}_{10},r^{(i)}_{30})\right]\right\}^{1/2};$$
$$i=1,2. \quad (2.40)$$

Modifying Eqs. (2.33) and (2.34) according to these definitions, they can be written in the following form:

$$\left\{\mathbf{I}_1\left[\frac{\partial^2}{\partial R^2}-\frac{l(l+1)}{R^2}\right]+\mathbf{k}^{(2)}_1-\mathbf{W}_1\right\}\Psi_{1m_0}-\mathbf{V}_{12}\Psi_{2m_0}=0, \quad (2.41)$$

$$\left\{\mathbf{I}_2\left[\frac{\partial^2}{\partial R^2}-\frac{l(l+1)}{R^2}\right]+\mathbf{k}^{(2)}_2-\mathbf{W}_2\right\}\Psi_{2m_0}-\mathbf{V}_{12}\Psi_{1m_0}=0,$$

where Ψ_{im_0} are column vectors related to the ith surface. We added the index m_0 to emphasize the fact that Eqs. (2.41) are solved for a given initial state (n_{10i_0},n_{30i_0}) where n_{10i_0} is the n_{10} vibrational state of the first diatomic, and n_{30i_0} is the n_{30} vibrational state of the second diatomic, both starting the interaction while they are on the surface i_0. Assuming that we include N_{1i} vibrational states of the first diatomic and N_{3i} vibrational states of the third diatomic, both for surface i, the dimensions of $\mathbf{I}_i$, $\mathbf{k}^{(2)}_i$, and $\mathbf{W}_i$ are $=(N_{1i}N_{3i})\times(N_{1i}N_{3i})$ and the dimensions of $\mathbf{V}_{12}$ are $(N_{11}N_{31})\times(N_{12}N_{32})$.

In order to calculate Ψ_{im_0}, one usually must determine all $2N$ independent solutions of Eqs. (2.41), where $N=N_{11}N_{31}+N_{12}N_{32}$. However, since only N of them behave correctly at the origin, we need to calculate only N solutions and consequently Eq. (2.41) becomes

$$\left[\mathbf{I}_1\left(\frac{\partial^2}{\partial R^2}-\frac{l(l+1)}{R^2}\right)+\mathbf{k}^{(2)}_1-\mathbf{W}_1\right]\Psi_1-\mathbf{V}_{12}\Psi_2=0,$$
$$\left[\mathbf{I}_2\left(\frac{\partial^2}{\partial R^2}-\frac{l(l+1)}{R^2}\right)+\mathbf{k}^{(2)}_2-\mathbf{W}_2\right]\Psi_2-\mathbf{V}_{12}\Psi_1=0,$$
$$(2.41')$$

where Ψ_i is a rectangular matrix of dimensions $(N_{1i}N_{3i})\times(N_{1i}N_{3i})$.

As mentioned above, Eqs. (2.41') are solved by propagation. The propagation is started at (or near) the origin, where the matrix elements of Ψ_i, $i=1,2$ are assumed to have finite (but otherwise arbitrary) values, and is continued out to the asymptotic region. The whole integration range is divided into sectors and two stages are distinguished:

(a) The integration, which is done in each sector by employing the Numerov method,[31] a method as easily implemented for the complex as for the real potentials.

(b) The transition from sector 1 to sector 2, which is done by employing the overlap matrices:

$$\Psi_i(R,\bar{R}_2)=\mathbf{S}^{(1,2)}_i\Psi_i(R,\bar{R}_1);\quad i=1,2, \quad (2.42)$$

where

$$\langle n_{1i}n_{3i}|S^{(1,2)}_i|n'_{1i}n'_{3i}\rangle=\langle n_{1i}|s^{(1,2)}_i|n_{1i}\rangle\langle n_{3i}|s^{(1,2)}_i|n'_{3i}\rangle;$$
$$i=1,2 \quad (2.43)$$

and

$$\langle n_{ji}|s^{(1,2)}_i|n'_{ji}\rangle=\int dr_j\,\phi^{(i)}_{n_{ji}}(r_j|\bar{R}_1,r^{(i)}_{j,01})\phi^{(i)}_{n'_{ji}}(r_j|\bar{R}_2,r^{(i)}_{j,02});$$
$$j\neq j';\quad i=1,2. \quad (2.44)$$

This completes our treatment of the SE.

E. Probabilities and cross sections

Once Eqs. (2.41') are solved, both the reactive and the CT probabilities can be calculated. First, we shall discuss the calculation of the reactive transition probabilities. As mentioned in the Introduction, the system has seven different arrangements. Since all atoms are similar, we have in fact two different kinds of reactive products:

$$H_2+H_2^+\rightarrow H_3^++H \quad (A)$$

and

$$HH'+H''H^+\rightarrow HH''+H'H^+. \quad (B)$$

Since reaction (A) is highly exothermic, whereas (B) is thermoneutral, it seems that H_3^+ is by far the preferred product. This preference is also supported by the TSH calculations.[10,11] Thus, to a very good approximation, it can be as-

sumed that the rupture of any bond of either H_2 or H_2^+ leads to (H_3^+, H) products, or, in other words, although there are six different exchange arrangements, only one kind of products is encountered. Next, according to the present method, we calculate only state-to-state nonreactive probabilities, and therefore, if the sum of all possible nonreactive probabilities is P_{ie}, then the reactive probability P_r is given simply by the relation

$$P_r = 1 - P_{ie}. \tag{2.45}$$

Thus, if $P_r(E_t l\gamma_1\gamma_3\phi|q_i v_{1i} v_{3i})$ is defined as the reactive transition probability for a given configuration (γ_1,γ_3,ϕ), for a given translational energy E_t, for a given angular momentum quantum number l, for a given initial surface q_i, and for given initial vibrational states (v_{1i},v_{3i}), then

$$P_r(E_t l\gamma_1\gamma_3\phi|q v_{1i} v_{3i}) = 1 - \sum_{q_f v_{1f} v_{3f}} |S(E_t l\gamma_1\gamma_3\phi|q_i v_{1i} v_{3i} q_f v_{1f} v_{3f})|^2, \tag{2.46}$$

where the summation is done with respect to all (asymptotic) open states. Here, $S(E_t l\gamma_1\gamma_3\phi|q_i v_{1i} v_{3i} q_f v_{1f} v_{3f})$ is the corresponding **S** matrix element which is obtained once Eq. (2.41′) is solved and the matching with the relevant asymptotic (physical) representation of the wave function is carried out. Since the calculations are done for a complex potential, we derive the **S** matrix elements directly, without going through an **R** matrix calculation.

Now, to calculate the reactive cross sections, we need to sum the l-weighted probabilities over all l values and integrate over the three angles (γ_1,γ_3,ϕ). Whereas no essential difficulties are encountered for the summation over l, the integration over the three angles is very time consuming. We therefore performed the integration employing the Monte Carlo method with respect to these angles.[30] Thus, we solved Eqs. (2.41′) for 28 different sets of angles (γ_1,γ_3,ϕ), which were obtained from a random distribution. If (x_1,x_2,x_3) are the three randomly selected numbers in the range [0,1], then the corresponding (γ_1,γ_3,ϕ) follow from the relations:

$$\gamma_1 = \cos^{-1}(2x_1 - 1),$$
$$\gamma_3 = \cos^{-1}(2x_2 - 1),$$
$$\phi = \pi x_3. \tag{2.47}$$

To obtain (x_1,x_2,x_3), we employed a computer subroutine which generates random numbers.

If $P(E_t l|q_i v_{1i} v_{3i} q_f)$ is the average inelastic transition probability (either with CT or without CT), which is calculated from the expression

$$P(E_t l|q_i v_{1i} v_{3i} q_f) = \sum_{v_{1f} v_{3f}} \sum_{x_1 x_2 x_3} |S(E_t l\gamma_1\gamma_3|q_i v_{1i} v_{3i} q_f v_{1f} v_{3f})|^2 \tag{2.48}$$

[here the summation over $(x_1 x_2 x_3)$ means the summation over all the randomly selected values] then the corresponding average l-dependent reactive probability is

$$P_r(E_t l|q_i v_{1i} v_{3i}) = 1 - \sum_{q_f} P(E_t l|q_i v_{1i} v_{3i} q_f). \tag{2.49}$$

The two final magnitudes to be considered are the total CT and total integral reactive cross sections. Thus, if

$$\sigma(E_t|q_i v_{1i} v_{3i} q_f) = \frac{\pi}{k^2_{q_i v_{1i} v_{3i}}} \times \sum_{l=0}^{l_m} (2l+1) P(E_t l|q_i v_{1i} v_{3i} q_f) \tag{2.50}$$

then

$$\sigma_{CT}(E_t|q_i v_{1i} v_{3i}) = \sigma(E_t|q_i v_{1i} v_{3i} q_f \neq q_i) \tag{2.51}$$

and

$$\sigma_r(E_t|q_i v_{1i} v_{3i}) = \frac{\pi(l_m+1)^2}{k^2_{q_i v_{1i} v_{3i}}} - \sum_{q_f} \sigma(E_t|q_i v_{1i} v_{3i} q_f). \tag{2.52}$$

This completes the theoretical section.

III. THE NUMERICAL TREATMENT

Our main concern in the numerical treatment is related to the parameters which define the NIDP. In one of our previous publications[15] we show that they can be determined *a priori* by employing the inequalities of Eq. (2.24). Here, we follow the same procedure and obtain that

$$u_{I0} = 1.0 \text{ eV}, \quad r_I = 2.5 \text{ Å}, \quad \Delta r_I = 1.5 \text{ Å}.$$

It should be emphasized that changing these parameters moderately will hardly affect the results. For instance, assuming u_{I0} to be 2 eV instead of 1 eV (or even 3 eV) had little impact on any of the final results.

The calculations were done for 28 different configurations, characterized by a set of randomly selected angles $(\gamma_{12},\gamma_{34},\phi)$. In all calculations we assumed the initial distance between the two diatomics R_{max} to be 5 Å and the smallest distance R_{min} to be 1.5 Å. As for the range of r (for the two diatomics), we assumed it to be $0.45 \leqslant r \leqslant 4$ Å.

The calculations were done for two values of total energy, $E_{tot} = 0.65, 0.91$ eV. Since the two lowest eigenvalues of H_2 (v) and H_2^+ (v^+) are

$$E_v = 0.261, \quad 0.782 \text{ eV}$$
$$E_{v^+} = 0.130, \quad 0.407 \text{ eV},$$

we have at most two open states (see Table I; the corresponding translational energies are also listed there). Although for the second energy two open states are encountered, namely $(v = v^+ = 0)$ and $(v = 0,\ v^+ = 1)$, we report results for the lower state only. In order to obtain reliable results for the vibrational excited state, we would have had to increase the value of R_{max} to 6.5 Å. Such an increase would have prevented us from completing the calculation with the available computer.

TABLE I. Translational energies in the $H_2 + H_2^+$ system (eV).

$E_v \setminus E_{tot}$	0.650	0.910
0.391	0.259	0.519
0.668	...	0.242

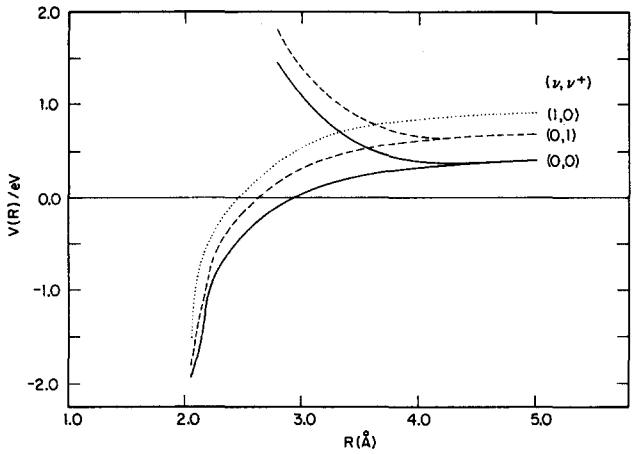

FIG. 5. The vibronic curves for the two lowest adiabatic–diabatic surfaces, as a function of the translational coordinate. The numbers (v,v^+) on the right-hand side are the vibrational quantum numbers for H_2 and H_2^+, respectively.

In the calculation we incorporated 46 vibrational states, which were distributed in the following way: For the H_2^+ molecule we included seven states on the lower surface and six on the upper; for the H_2 molecule four states were included on the lower surface and three on the upper. Increasing these numbers had hardly any effect on the resulting probabilities and no effect on the final cross sections.

The SE was solved for every second l value (namely, for even l values only); the largest value of l, i.e., l_m, was 56 for the lower energy and 78 for the higher energy. To get cross sections, the missing probabilities were interpolated. This procedure is not expected to affect the final reactive and/or CT cross sections.

IV. RESULTS

Although we are dealing with only one type of reagent, namely $H_2 + H_2^+$, we must still consider (at least) two potential surfaces (which coincide asymptotically) and distinguish between the reagents moving on the lower surface and those moving on the upper. These two surfaces are coupled, so that quantum mechanically, the two kinds of reagents are treated in one single calculation and the distinction between the two types follows from this calculation. As described in Sec. II, the treatment of the adiabatic surfaces and the corresponding nonadiabatic coupling terms leads to the (potential) coupled adiabatic–diabatic surfaces. There are different ways to show the relationship between these two surfaces. Quantum mechanically, this is best represented by the vibronic curves. In Fig. 5 we show the vibronic curves for a strongly reactive configuration, namely, $\gamma_{12} = 0°$, $\gamma_{34} = 90°$. It can be seen that the coupling between the two surfaces produces one attractive and one repulsive surface and that, asymptotically, the two surfaces coincide.

As was mentioned earlier, the QM calculations were done for two energies: $E_{tot} = 0.65, 0.91$ eV. For each of these two energies we report on results for the lower vibrational state only; one (total) cross section (CS) for reaction and one for CT. In Table II are presented all final integral QM-CS's, those for each surface separately and the final ones (obtained by taking the average between the two). It can be seen that, in general, the CS's obtained for the two surfaces are reasonably close. However, whereas the CT-CS's must be identical because of the Hermitianity of the S matrix (the slight differences are mainly due to the R_{max} values not being large enough), there is, to our knowledge, no first principle which compels the two corresponding reactive CS's to be identical.

A comparison of our results with the results of the TSH treatment and with the experimental results is presented in Table III. Since the available TSH CS's were obtained for the lower surface only, the QM results which we show in the table are given for the lower surface. The main findings are as follows:

(a) Compared with the TSH results, the QM reactive CS's are much smaller, while the CT-CS's are much larger.

(b) Compared with experiment, again the reactive CS's are smaller, but this time the discrepancy is not as large: about 15% for the lower energy and 35% for the higher.

The discrepancy between theory and experiment is not too disturbing because it could follow from the choice of the potential used in the calculation, which may not be the most appropriate one. However, the discrepancy between the two

TABLE II. Total quantum mechanical cross section (Å^2) for reaction and charge transfer.

	E_{tot} (eV)	0.65	0.91
	E_{tr} (eV)	0.252	0.519
	Initial vib. state	(0,0)	(0,0)
Reaction	Lower surface	28.0	19.3
	Upper surface	24.4	17.1
	Average	26.2	18.2
Charge transfer	Lower surface	15.2	14.2
	Upper surface	15.4	15.5
	Average	15.3	14.8

TABLE III. Reactive and charge transfer cross sections (Å^2) (lower surface results only).

	E_{tot} (eV)	0.65	0.91
	E_{tr} (eV)	0.252	0.519
	Initial vib. state	(0,0)	(0,0)
Reaction	QM	28	19
	SCL[a,b]	46 ± 1	30 ± 1
	EXP[c]	34 ± 2	26 ± 1
Charge transfer	QM	15	14
	SCL[b]	3.9 ± 0.5	9 ± 1

[a] Reference 11.
[b] Reference 9(c).
[c] Reference 6.

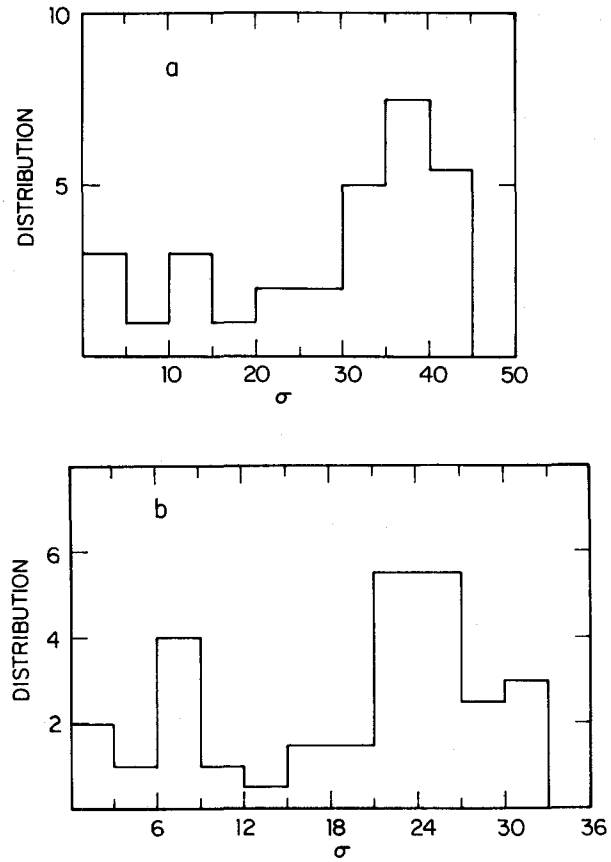

FIG. 6. The distribution function of the reactive cross sections calculated for 28 randomly selected angular configurations ($\gamma_{12}, \gamma_{34}, \phi$). (a) The distribution for $E_{tot} = 0.65$ eV ($E_{tr} = 0.259$ eV). (b) The distribution for $E_{tot} = 0.91$ eV ($E_{tr} = 0.519$ eV).

numerical treatments is much more serious. We shall devote the rest of this paper to this issue.

Except for the obvious fact that one treatment is semiclassical (SCL) and the other QM, another difference is in that the SCL treatment is "exact," whereas the QM is approximate. We shall show in the next section that the main reason for the discrepancy between the results lies not in the use of the IOSA but rather in the fact that the SCL treatment does not fully take into account the behavior of the two interacting molecules H_2 and H_2^+.

V. DISCUSSION

This section is divided into two main parts, one devoted to the reactive CS and the other to the CT-CS.

A. The reaction process: $H_2 + H_2^+ \rightarrow H_3^+ + H$

The IOSA treatment was carried out for 28 sets of randomly chosen angles ($\gamma_{12}, \gamma_{34}, \phi$). The distribution of the calculated CS (assuming each of these sets of three angles yields the correct CS) is shown in Fig. 6; Fig. 6(a) shows the results for $E_{tr} = 0.252$ eV and Fig. 6(b) for $E_{tr} = 0.519$ eV. The distributions are presented in the form of histograms. In Fig. 6(a), for instance, the first column means that three sets of angles produced CS's in the range [0, 5 Å^2], etc.

The main findings are:

(a) Most of the randomly chosen angular configurations lead to large CS's, but still a not negligible number of them yield smaller and sometimes even very small CS's.

(b) The distributions obtained for the two energies are rather different. As the energy goes up, the frequency of the extremal cases (namely, either very large or very small CS's) decreases significantly.

The results in Fig. 6 reveal one of the main reasons for the much smaller QM CS's, namely, that a relatively large number of the (frozen) angular configurations yield relatively small reactive CS's. However, the results also indicate that there is not even one single configuration which yields a CS that comes close to the (average) SCL-CS. For instance, in case of $E_{tr} = 0.259$ eV, the SCL-CS is 46 Å^2, whereas the largest CS encountered in our calculations is 41.9 Å^2 (obtained for $\gamma_{12} = 175°, \gamma_{34} = 59°, \phi = 148°$). It should be emphasized that we also conducted a search for larger CS's, but we did not find any. The CS for the configuration ($\gamma_{12} = 0°, \gamma_{34} = 90°, \phi = 0°$), for instance, yields $\sigma = 39.2$ Å^2 only.

The findings which we present here are obviously quite discouraging, but it appears that the situation is in fact even more serious. The published SCL result is for the reaction

$$H_2(v = 0, j = 1) + H_2^+(v^+ = 0, j^+ = 2) \rightarrow H_3^+ + H,$$

whereas our calculations were done for $j = j^+ = 0$. According to unpublished results,[32] the SCL-CS for $j = j^+ = 0$ is even larger, namely, $\sigma = 53.2$ Å. Thus, the question which must be asked is why all the QM CS's are relatively so small. To answer this, we present in Fig. 7 the reactive transition probabilities as a function of the orbital angular momental quantum number l; the results for $E_{tr} = 0.259$ eV are shown in Fig. 7(a) and those for $E_{tr} = 0.519$ eV are shown in Fig. 7(b). In each figure are given four curves, two of which represent the average of all 28 configurations; one curve is for the lower surface, and the other for the upper surface. In addition are shown the (lower surface) probability curves for two selected configurations; one for $\gamma_{12} = 0°$, $\gamma_{34} = 90°$, $\phi = 0°$ and the other for $\gamma_{12} = 0°$, $\gamma_{34} = 10°$, $\phi = 0°$. The latter is an almost collinear configuration.

The main findings are as follows:

(a) Three curves show a relatively weak dependence on l and only the collinear curve exhibits a more pronounced dependence.

(b) As expected, the largest probabilities are obtained for the $\gamma_{12} = 0°$, $\gamma_{34} = 90°$ configuration; they are significantly larger than the average probabilities.

(c) All probabilities become identically zero for $l > 46$, which corresponds to the impact parameter $b = 4.1$ Å.

The results presented in Fig. 7(a) show that the lower potential energy surface (which follows from the adiabatic–diabatic transformation) cannot yield, for any configuration, the large SCL CS. Moreover, even assuming $P(l) = 1$ for $0 \leqslant l \leqslant 46$ will lead to a CS of 52.8 Å^2, which is still lower than the SCL-CS of 53.2 Å^2.

The conclusion from the above analysis is that the lower

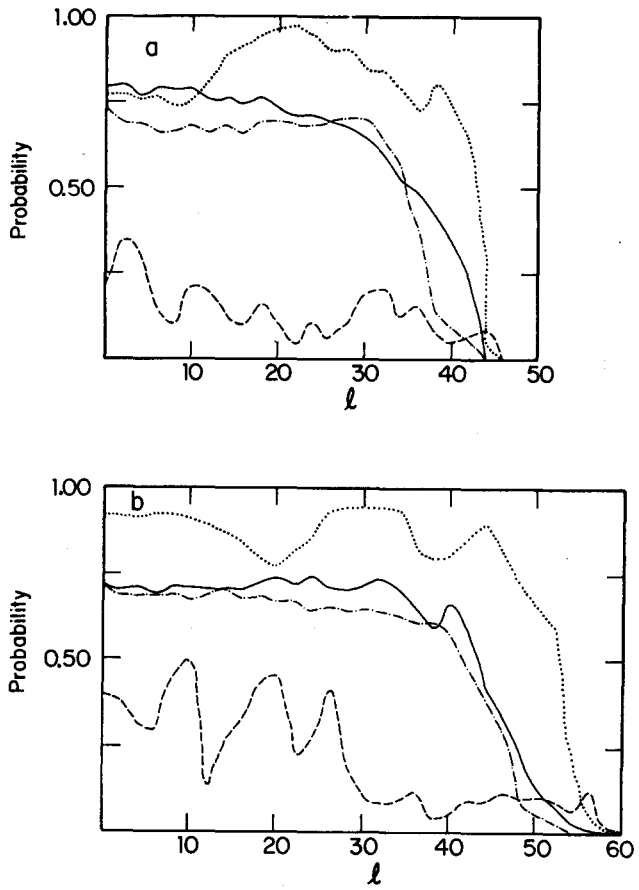

FIG. 7. The reactive probabilities as a function of the orbital angular quantum number l. —, Average probabilities (lower surface); –·–, average probabilities (upper surface); ···, probabilities for the fixed configuration ($\gamma_{12}=0°, \gamma_{34}=90°$); ---, probabilities for the fixed configuration ($\gamma_{12}=0$, $\gamma_{34}=10°$). (a) Results for $E_{tot}=0.65$ eV ($E_{tr}=0.259$ eV). (b) Results for $E_{tot}=0.91$ eV ($E_{tr}=0.519$ eV).

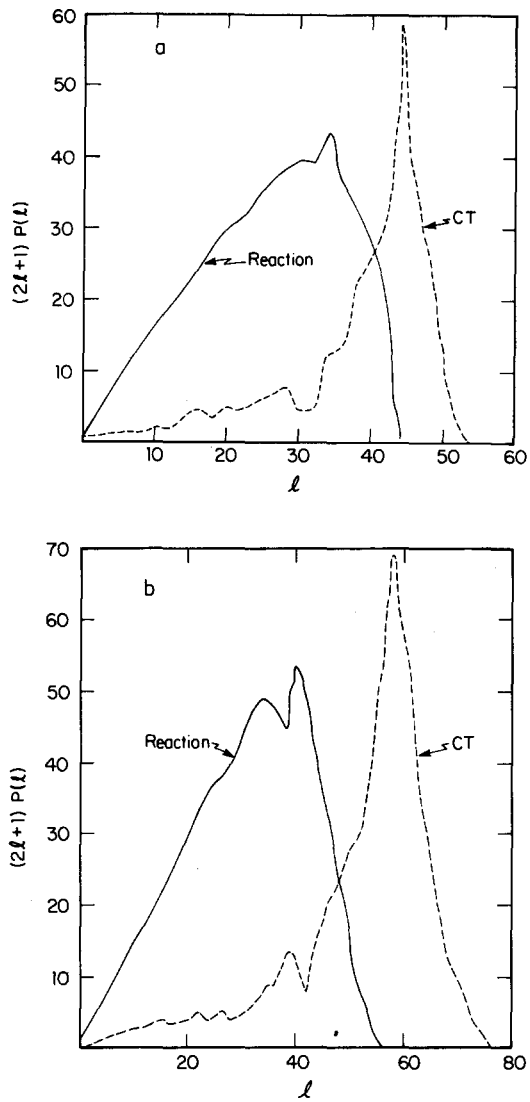

FIG. 8. Average (lower surface) opacity functions for reaction and charge transfer. (a) $E_{tot}=0.65$ eV ($E_{tr}=0.259$ eV); (b) $E_{tot}=0.91$ eV ($E_{tr}=0.519$ eV).

adiabatic surface employed in the SCL calculation probably decreases much faster, as a function of the translational coordinate, than does the lower surface due to the QM treatment. Therefore, larger l values are allowed to contribute to the SCL-CS, thus yielding larger reactive cross sections. This implies that the SCL results must be treated with some care. The reason that the surfaces employed in the QM treatment are not purely adiabatic (and therefore not so low) is that this treatment takes into account the nonadiabatic coupling terms, which are essentially ignored in the SCL treatment.

B. The charge transfer process: $H_2+H_2^+ \rightarrow H_2^+ + H_2$

In contrast to exchange CS's, CT-CS's for the energy range < 1 eV are scarce. The only available CS's are those published by Stine and Muckerman,[9(c)] which are supported by additional calculations by Eaker.[32] Whereas the reactive SCL-CS's are much larger than the QM-CS's, the SCL-CT-CS's are much smaller. This finding is not fortuitous; we found that whenever a certain (angular) configuration yields a smaller reactive CS, it will yield a large CT-CS, and *vice versa*. Apparently, there is a strong linkage between the two processes. To obtain a better understanding of this linkage, we present in Figs. 8 and 9 opacity functions [i.e., $(2l+1)P(l)$] for the two processes. In Fig. 8 are the results for the average of the 28 configurations and in Fig. 9 the results for the favorable reactive configuration ($\gamma_{12}=0°, \gamma_{34}=90°$). The results in Figs. 8(a) and 9(a) are for the lower energy, i.e., $E_{tr}=0.259$ eV, and those in Figs. 8(b) and 9(b) are for the higher energy, $E_{tr}=0.519$ eV. It can be seen from Fig. 8 that since the opacity functions for reaction are relatively small, those for the CT become relatively large. The opposite is seen in Fig. 9 where, due to the fact that the reactive opacity functions are large, the CT ones

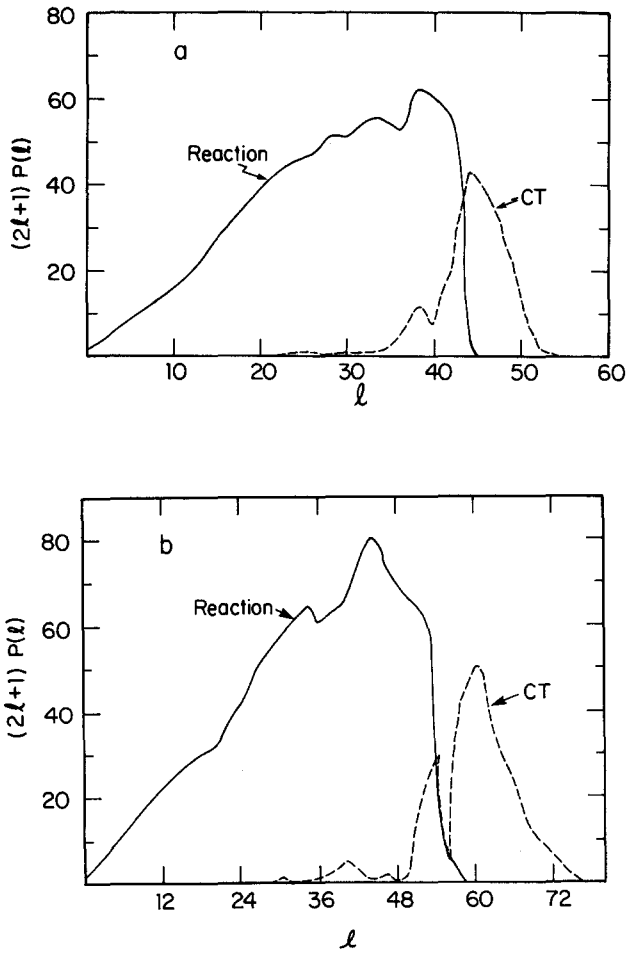

FIG. 9. Opacity functions for reaction and charge transfer for lower surface ($\gamma_{12} = 0°$, $\gamma_{34} = 90°$). For notation see Fig. 8.

become smaller. The fact that the reactive process affects so strongly the CT process indicates that the CT processes take place mainly while the two nonreactive species are receding. In classical terms, this implies that trajectories which do not lead to exchange finally yield the charge transfer. Thus, it is the reaction process which directly affects the size of the CT-CS.

The CT curves in Fig. 8 have another interesting feature, namely, the sharp peak at around $l \sim 44$ for the lower energy and $l \sim 57$ for the higher (the former l value corresponds to $b = 3.9$ Å and the latter to $b = 3.7$ Å). These sharp peaks could lead to a preferred scattering angle, which would eventually be experimentally detectable.

VI. SUMMARY

This work reports on the first QM treatment of $H_2 + H_2^+$ in the low energy region (< 1 eV), in which both the reaction process and the CT process are considered. The system was treated in its full dimensionality, without limiting any of the exchange or CT processes. The only constraints imposed were those associated with the three internal (orientational) angles, which were assumed to be constant while the SE was solved. The solution of the SE was carried out for 28 randomly selected sets of the three angles γ_{12}, γ_{34}, and ϕ (see Fig. 2). The resulting S-matrix elements were (absolutely) squared to become probabilities, which were then averaged to yield the probabilities for the various processes. The main conclusions are:

(1) The reactive and the CT processes are strongly coupled in this system. We found that the more enhanced the reactive process, the weaker is the CT process. In other words, the dominant process in this system is the reaction process.

(2) The calculated reaction cross sections are in reasonable agreement with the experimental results, but deviate significantly from the SCL reactive cross sections.

The main reason for the unusual discrepancy between the two theoretical treatments is associated with the potential energy employed in each treatment. The lower (reactive) surface in the SCL treatment is the lowest adiabatic surface, which decreases unusually fast as the distance between the two diatomics becomes smaller, thus allowing large impact parameters to contribute to the reactive cross section. The lower surface in the QM treatment is an adiabatic–diabatic surface, which is a kind of average between the *two* lower adiabatic surfaces, and which therefore decreases, as a function of the translation coordinate, at a much slower pace, so that contributions of the large impact parameters are excluded. This adiabatic–diabatic surface results from a theoretical treatment which takes into account the nonadiabatic coupling terms, which are entirely ignored in the SCL treatment. This fact led us to the conclusion that a revision of the SCL approach to treating charge transfer (and other electronic transitions) in heavy-particle collisions is called for.

This is only the first QM treatment for $H_2 + H_2^+$, this vast, complicated, and interesting system. More intensive theoretical studies and much more extensive calculations are needed to fully grasp its many beautiful features.

ACKNOWLEDGMENTS

This work was supported by the National Science Foundation Grant No. CHE 8913283. Acknowledgement is also made to the donors of the Petroleum Research Fund, administered by the American Chemical Society, for the partial support of this research. The theoretical computation was made possible by a grant from the Computer Center of Iowa State University and a grant from the Director Development Fund of the Ames Laboratory. One of the authors (M.B.) would like to thank Professor G. C. Schatz for making available to him the computer subroutine for calculating the H_4^+ DIM potential, Professor C. W. Eaker for providing him with a few of the unpublished cross sections, and the two of these colleagues for illuminating discussions. This author would also like to thank L. Versteegh, head of the Operation Department, and the operators of the Iowa State University Computer Center for their help in running the computer programs.

[1] B. G. Reuben and L. Friedman, J. Chem. Phys. **37**, 1636 (1962); C. F. Giese and W. B. Maier II, *ibid.* **39**, 739 (1963); A. Weingartshofer and E. M. Clarke, Phys. Rev. Lett. **12**, 591 (1964); M. Saporoschenko, J. Chem. Phys. **42**, 2760 (1965); D. W. Vance and T. L. Bailey, *ibid.* **44**, 486 (1966); L. D. Doverspike and R. L. Champion, *ibid.* **46**, 4718 (1967); L. Matus, I. Opauszky, D. Hyatt, A. J. Masson, K. Birkinshaw, and M. J. Henchman, Discuss. Faraday Soc. **44**, 146 (1967); J. J. Leventhal, T. F. Moran, and L. Friedman, J. Chem. Phys. **46**, 4666 (1967); J. Durup and M. Durup, *ibid.* **64**, 386 (1967); M. Yamane, *ibid.* **49**, 4624 (1968); W. A. Chupka, M. E. Russell, and K. Refaey, *ibid.* **48**, 1518 (1968); R. H. Neynaber and S. M. Trujillo, Phys. Rev. **167**, 63 (1968); T. F. Moran and J. R. Roberts, J. Chem. Phys. **49**, 3411 (1968); M. T. Bowers, D. D. Elleman, and J. J. King, Jr., *ibid.* **50**, 4787 (1969); A. Henglein, J. Phys. Chem. **76**, 3883 (1972); R. N. Stocker and H. Newmann, J. Chem. Phys. **61**, 3852 (1974); A. B. Lees and P. K. Rol, *ibid.* **61**, 4444 (1975); W. R. Gentry, D. J. McClure, and C. H. Douglass, Rev. Sci. Instrum. **46**, 367 (1975).

[2] I. Koyano and K. Tanaka, J. Chem. Phys. **72**, 4858 (1980).

[3] S. L. Anderson, F. A. Houle, D. Gerlich, and Y. T. Lee, J. Chem. Phys. **75**, 2153 (1981).

[4] J. R. Krenos, K. K. Lehmann, J. C. Tully, P. M. Hierl, and G. P. Smith, Chem. Phys. **16**, 109 (1976).

[5] C. L. Liao, C.-X. Liao, and C. Y. Ng, J. Chem. Phys. **81**, 5672 (1984); C. L. Liao and C. Y. Ng, *ibid.* **84**, 197 (1986).

[6] J. W. Shao and C. Y. Ng, J. Chem. Phys. **84**, 4317 (1986).

[7] H. Eyring, J. O. Hirschfelder, and H. S. Taylor, J. Chem. Phys. **4**, 479 (1936); D. R. Bates and R. H. G. Reid, Proc. R. Soc. London Ser. A **1**, 310 (1969); T. F. Moran, M. R. Flannery, and D. L. Albritton, J. Chem. Phys. **62**, 2869 (1975); M. R. Flannery, J. V. Hornstein, and T. F. Moran, Chem. Phys. Lett. **32**, 455 (1975); T. F. Moran, K. J. McCann, M. R. Flannery, and D. L. Albritton, J. Chem. Phys. **65**, 3172 (1976); C. Y. Lee and A. E. DePristo, *ibid.* **80**, 1116 (1984).

[8] F. A. Wolf and J. L. Haller, J. Chem. Phys. **52**, 5910 (1970).

[9] (a) J. R. Stine and J. T. Muckerman, J. Chem. Phys. **65**, 3975 (1976); (b) J. R. Stine and J. T. Muckerman, J. Chem. Phys. **68**, 185 (1978); (c) J. T. Muckerman, Theor. Chem. **6**, 1 (1981).

[10] C. W. Eaker, G. C. Schatz, N. DeLeon, and E. J. Heller, J. Chem. Phys. **81**, 5913 (1984); C. W. Eaker and G. C. Schatz, *ibid.* **81**, 2394 (1984); **89**, 2612 (1985); C. W. Eaker and J. L. Muzyka, Chem. Phys. Lett. **119**, 169 (1985).

[11] C. W. Eaker and G. C. Schatz, Chem. Phys. Lett. **127**, 343 (1986).

[12] D. Neuhauser and M. Baer, J. Chem. Phys. **90**, 4351 (1989).

[13] D. Neuhauser and M. Baer, J. Chem. Phys. **93**, 2862 (1989); J. Chem. Phys. **91**, 4651 (1989); D. Neuhauser, M. Baer, R. S. Judson, and D. J. Kouri, *ibid.* **90**, 5882 (1989); J. Chem. Phys. **93**, 312 (1990); Chem. Phys. Lett. **169**, 372 (1990); Comp. Phys. Commun. (in press); R. S. Judson, D. J. Kouri, D. Neuhauser, and M. Baer, Phys. Rev. A **42**, 351 (1990).

[14] D. Neuhauser and M. Baer, J. Phys. Chem. **94**, 185 (1990); J. Chem. Phys. **92**, 3419 (1990); M. Baer, D. Neuhauser, and Y. Oreg, Faraday Trans. **86**, 1721 (1990).

[15] D. Neuhauser, M. Baer, and D. J. Kouri, J. Chem. Phys. **93**, 2499 (1990).

[16] M. Baer, C. Y. Ng, and D. Neuhauser, Chem. Phys. Lett. **169**, 539 (1990).

[17] M. Baer, C.-L. Liao, R. Xu, G. D. Flesch, S. Nourbakhsh, C. Y. Ng, and D. Neuhauser, J. Chem. Phys. (in press).

[18] V. Khare, D. J. Kouri, and M. Baer, J. Chem. Phys. **71**, 1188 (1979); J. Jellinek and M. Baer, *ibid.* **76**, 4883 (1982); H. Nakamura, A. Ohsaki, and M. Baer, J. Chem. Phys. **90**, 6176 (1986). For other versions see, for instance, J. M. Bowman and K. T. Lee, J. Chem. Phys. **72**, 5071 (1980); M. Nakamura and H. Nakamura, *ibid.* **90**, 4853 (1989); B. M. D. Jepsen op de Haar and G. G. Balint-Kurti, *ibid.* **85**, 329 (1987); D. C. Clary and G. D. Drolshagen, *ibid.* **76**, 5027 (1982).

[19] Q. Sun and J. M. Bowman, J. Chem. Phys. **92**, 1021, 5201 (1990); A. N. Brooks and D. C. Clary, *ibid.* **92**, 4178 (1990).

[20] R. Polak, Chem. Phys. **16**, 353 (1976).

[21] F. O. Ellison, J. Am. Chem. Soc. **85**, 3540 (1963); P. J. Kuntz, in *Theory of Chemical Reaction Dynamics, Vol. I*, edited by M. Baer (CRC, Boca Raton, 1985), Chap. 2.

[22] M. Baer, Chem. Phys. Lett. **35**, 112 (1975); Chem. Phys. **15**, 49 (1976).

[23] M. Baer, in *Theory of Chemical Reaction Dynamics, Vol. II*, edited by M. Baer (CRC, Boca Raton, 1985), Chap. 4.

[24] R. K. Preston and J. C. Tully, J. Chem. Phys. **54**, 4297 (1971).

[25] M. Baer, G. Niedner-Schatteburg, and J. P. Toennies, J. Chem. Phys. **88**, 1461 (1988); **91**, 4169 (1989).

[26] M. Baer, H. Nakamura, and A. Ohsaki, Chem. Phys. Lett. **131**, 468 (1986); M. Baer and H. Nakamura, J. Chem. Phys. **87**, 465 (1987). For earlier work see M. Baer and A. J. Beswick, Chem. Phys. Lett. **51**, 369 (1977); Phys. Rev. A **19**, 1559 (1979).

[27] M. Baer, G. Niedner-Schatteburg, and J. P. Toennies, Chem. Phys. Lett. **167**, 269 (1990).

[28] F. T. Smith, Phys. Rev. **179**, 111 (1969).

[29] S. Green, J. Chem. Phys. **70**, 816 (1979); R. Goldflam and D. J. Kouri, *ibid.* **70**, 5076 (1976); D. C. Clary, *ibid.* **75**, 2899 (1981).

[30] B. R. Johnson, J. Chem. Phys. **84**, 176 (1986).

[31] M. A. Abramowitz and I. A. Stegun, *Handbook for Mathematical Functions* (NBS, Washington, D.C., 1964), p. 897 (the formula appears under Milne *C* Method).

[32] C. W. Eaker (private communication, this calculation was only recently completed for the purpose of this comparison).